DOI: 10.1002/ejic.200601077

Alternative Synthesis, Density Functional Calculations and Proton Reactivity Study of a Trinuclear [NiFe] Hydrogenase Model Compound

Frank Lauderbach,[a] Raju Prakash,*[a][‡] Andreas W. Götz,*[b][‡‡] Marcela Munoz,[b] Frank W. Heinemann,[a] Ulrich Nickel,[b] Bernd A. Hess,[c][†] and Dieter Sellmann[a][†]

Keywords: Constant potential coulometry / Density functional calculations / Iron / Nickel / NiFe hydrogenases / S ligands

The trinuclear complex [('S_2')\{Ni(PMe_3)\}$_2$Fe(CO)('S_2')$_2$] (**1**) {'S_2'$^{2-}$ = 1,2-benzenedithiolate(2–)} has been reported as a structural as well as functional model for [NiFe] hydrogenases since it contains key structural features of the [NiFe] hydrogenase active site, and is oxidized by protons to give [**1**]$^+$ and H_2. Complex **1** formed as an unexpected product from the reaction of [Fe(CO)$_2$('S_3')]$_2$ {'S_3'$^{2-}$ = bis(2-mercaptophenyl) sulfide(2–)} and [Ni(PMe_3)$_2$('S_2')]. Both the iron and nickel centers of **1** are chelated by 'S_2' donors, but not with any 'S_3' ligand. In order to understand this reaction, the new precursor [Fe(CO)$_2$($^{si}S_3$)]$_2$ (**2**) {$^{si}S_3^{2-}$ = bis(2-mercapto-3-trimethylsilylphenyl) sulfide(2–)} was synthesized. Compound **2** readily loses its CO ligand to give [Fe(CO)($^{si}S_3$)]$_2$ (**3**), which consists of two 16 valence electron fragments and could be isolated in the solid state. Conversion of **3** to **2** is feasible with gentle bubbling of CO gas for about 2 min. Treatment of **2** with [Ni(PMe_3)$_2$('S_2')] resulted exclusively in the formation of complex **1**, which confirms that all three 'S_2' ligands in **1** originate from [Ni(PMe_3)$_2$('S_2')]. Therefore, an alternative synthesis of **1**, which does not involve any 'S_3' ligand, has been developed. Density functional theory (DFT) calculations suggest that the oxidation states of the metal centers are Fe^{II} and Ni^{II} and do not change upon oxidation of **1** to [**1**]$^+$. The unpaired electron in [**1**]$^+$ is located to a large extent on the nickel atoms and the adjacent thiolate donor functions. The charge, however, is distributed over the whole cluster, main parts residing on the 'S_2' ligands. Preliminary constant potential coulometric measurements indicate that **1** mediates the reduction of protons to dihydrogen at a mild potential (–0.48 V vs. NHE). Based upon these experimental and theoretical results, plausible mechanisms for this reduction are briefly discussed.

Introduction

Hydrogenases comprise a fundamental group of bacterial enzymes that catalyze the reversible interconversion of protons and molecular hydrogen. Thus, they play a key role in molecular bioenergetics.[1] In recent years, interest in hydrogenases has intensified due to their environmental and industrial potential in the context of the development of a pollution-free and sustainable hydrogen economy.[2] Hydrogenases can be divided into two main groups based on the type of metal containing active sites, namely, [NiFe][3] and [Fe]-only[4] hydrogenases. [NiFe] hydrogenases represent the major class among hydrogenases, consisting of a dinuclear nickel–iron active site (Figure 1).

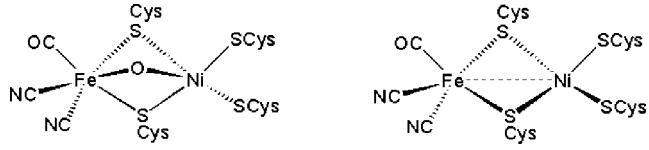

Figure 1. Schematic structures of the active sites of [NiFe] hydrogenases. Left: oxidized form from *D. gigas.*[3a,3b] Right: Reduced form from *D. vulgaris* Miyazaki.[3d]

Numerous spectroscopic,[5] structural,[3,6] and theoretical[7] studies on various enzymes have provided further insight into the structure and function of the active sites of [NiFe] hydrogenases. Despite these efforts, the exact nature of the catalytic cycle and the exact oxidation state of nickel during the catalytic cycle remain uncertain. This has prompted the synthesis of a number of low-molecular weight di- and oligonuclear heterometallic complex analogues to the active site of the [NiFe] enzymes.[8,9] Studies on such compounds can lead to a better understanding of the properties of the active site and can shed light on the catalytic reaction that takes place in the enzyme. The advantage of such models is that they are low-molecular

[a] Institut für Anorganische Chemie der Universität Erlangen-Nürnberg,
Egerlandstrasse 1, 91058 Erlangen, Germany
Fax: +49-9131-852-1165
E-mail: raju.prakash@chemie.uni-erlangen.de
[b] Institut für Physikalische und Theoretische Chemie der Universität Erlangen-Nürnberg,
Egerlandstrasse 3, 91058 Erlangen, Germany
[c] Lehrstuhl für Theoretische Chemie der Universität Bonn,
Wegelerstrasse 12, 53115 Bonn, Germany
[‡] Present address: Institut für Organische Chemie der Universität Erlangen-Nürnberg, Henkestrasse 42, 91054 Erlangen, Germany.
[‡‡] Present address: Department of Theoretical Chemistry, Faculty of Sciences, Vrije Universiteit Amsterdam, De Boelelaan 1083, 1081 HV Amsterdam, The Netherlands;
E-mail: agoetz@few.vu.nl
[†] Deceased.

weight compounds and therefore are often more easily isolated and examined by various physicochemical methods than the macromolecular enzyme itself. In addition, electronic and steric modifications can be generated by adjusting the ligand environment.

Recently, two [NiFe] model complexes $[Fe(CO)_2(CN)_2(\mu\text{-}SCH_2CH_2CH_2S)Ni(S_2CNR_2)]$ [R = Et and -$(CH_2)_5$-] were synthesized which up to now resemble the structural features of hydrogenases most closely.[10] However, in practice, none of the reported sulfur-bridged [NiFe] model complexes shows any hydrogenase-like reactivity.

We have previously reported on the sulfur-bridged trinuclear complex [('S_2')\{$Ni(PMe_3)$\}$_2$Fe(CO)('S_2')$_2$] (**1**) {'S_2'$^{2-}$ = 1,2-benzenedithiolate(2–)}, which stoichiometrically reduces protons to dihydrogen and in turn gets oxidized to [('S_2')\{$Ni(PMe_3)$\}$_2$Fe(CO)('S_2')$_2$]$^+$ ([**1**]$^+$).[11] The reversible conversion of **1**/[**1**]$^+$ was also achieved with ferrocenium salt and NBu_4BH_4, respectively. Moreover, the structural parameters (bond lengths and angles) of **1** and [**1**]$^+$ are nearly identical. This structural rigidity during the redox reaction indicates a low reorganization barrier and therefore favors a rapid electron transfer.[12] This result is insofar highly interesting as many oxidoreductases undergo redox reactions which are accompanied only by marginal structural changes. These intriguing facts inspired us to investigate the properties of **1** in greater detail. Herein, we describe the exact formation pathway and a novel straightforward synthetic route of **1**. Density functional Theory (DFT) calculations reveal important insights into the oxidation reaction of **1** to [**1**]$^+$. In addition, we report preliminary coulometric studies which employed **1** as an electrocatalyst for the reduction of protons to dihydrogen at a low reduction potential.

Results and Discussion

Synthesis

It has already been reported that the trinuclear NiFe complex **1** formed by the reaction of [Fe(CO)$_2$('S_3')]$_2$ {'S_3'$^{2-}$ = bis(2-mercaptophenyl) sulfide(2–)} with [$Ni(PMe_3)_2$('S_2')] according to Scheme 1.[11] In this reaction compound **1** was the only isolated product with 18% yield (it is not possible to give the exact stoichiometry for Scheme 1, however, the given numbers denote only the ratio of the initial reactants used). Both the iron as well as the nickel coordination centers of **1** are chelated by 'S_2' donors, but surprisingly not with any 'S_3' ligand. Therefore, it is interesting to know how **1** can be formed from the reactants in which the Fe center is not bearing any 'S_3' ligand. We can think about two possible pathways for the formation of **1**: in the first route, an initial reductive cleavage of the 'S_3' ligand at the iron center to an 'S_2' ligand and subsequent reaction of this intermediate species with [$Ni(PMe_3)_2$('S_2')] to form **1**; in the second route, a ligand exchange type of reaction in which all 'S_2' ligands originate from the reactant [$Ni(PMe_3)_2$('S_2')]. If **1** would be formed via the reductive cleavage pathway, the use of a derivatized 'S_3' ligand in the dinuclear iron precursor complex should result in a new trinuclear NiFe complex containing at least one derivatized 'S_2' ligand. Conversely if the reaction proceeded via a ligand-exchange pathway, the use of a derivatized 'S_3' ligand in the dinuclear iron precursor complex should result in exclusively the trinuclear complex **1**. Herein we have chosen the twofold silylated derivative of the 'S_3' ligand, $^{si}S_3$–H_2 {$^{si}S_3^{2-}$ = bis(2-mercapto-3-trimethylsilylphenyl) sulfide(2–)}, for the synthesis of the derivative of the [Fe(CO)$_2$('S_3')]$_2$ precursor. Since the $SiMe_3$ group is a good NMR probe, it enables the detection of the reaction pathway of the formation of **1**.

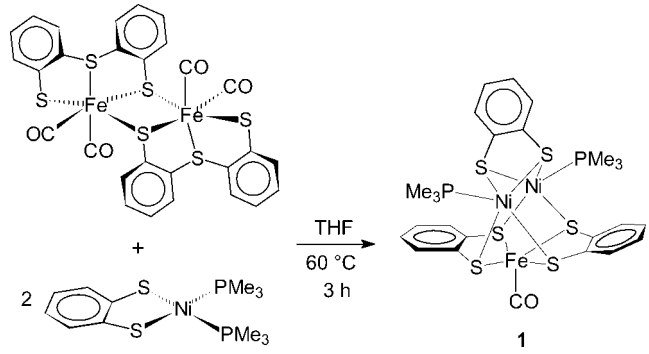

Scheme 1. Synthesis of complex **1**.

The silylated precursor complex [Fe(CO)$_2$($^{si}S_3$)]$_2$ (**2**) was prepared similarly to the synthesis of the unsubstituted parent compound as reported in the literature,[13] except that the reaction was performed under CO atmosphere. Addition of the ligand $^{si}S_3$–H_2 to [Fe(bda)(CO)$_3$] (bda = benzylideneacetone) in THF led to a dark green solution and gas evolution. Keeping this solution at –20 °C for two weeks, brown crystals suitable for X-ray structure analysis were obtained. The molecular structure of **2** is shown in Figure 2 and selected bond lengths and bond angles are given in Table 1. The structural parameters of the silylated centrosymmetric compound **2** differ only marginally from the parent compound [Fe(CO)$_2$('S_3')]$_2$.[13] Complex **2** consists of two distorted octahedral fragments that are linked by an edge. Within these fragments, the thiolate donors are *cis* to each other. One CO is coordinated *trans* to a bridging thiolate S atom, whereas the other CO is in *trans* position to the thioether S donor. The distances around Fe, including Fe–CO bonds, are in the range usually found for diamagnetic octahedral thiolate-thioether complexes.[12] The Fe–thiolate bond lengths are longer than the Fe–thioether bond lengths. The Fe–Fe distance of 341.51(6) pm indicates that there is no metal–metal interaction.

Compound **2** is diamagnetic and sparingly soluble in most common solvents. However, it is better soluble than the unsubstituted derivative. It is stable in CO saturated solvents for about two weeks. On prolonged standing, it gradually decomposes to form a stable five-coordinate dinuclear species [Fe(CO)($^{si}S_3$)]$_2$ (**3**).

The molecular structure of **3** is depicted in Figure 3 and selected bond lengths and angles are given in Table 1. The molecule can be described as two edge-linked distorted trigonal bipyramids. It contains two 16 valence electron frag-

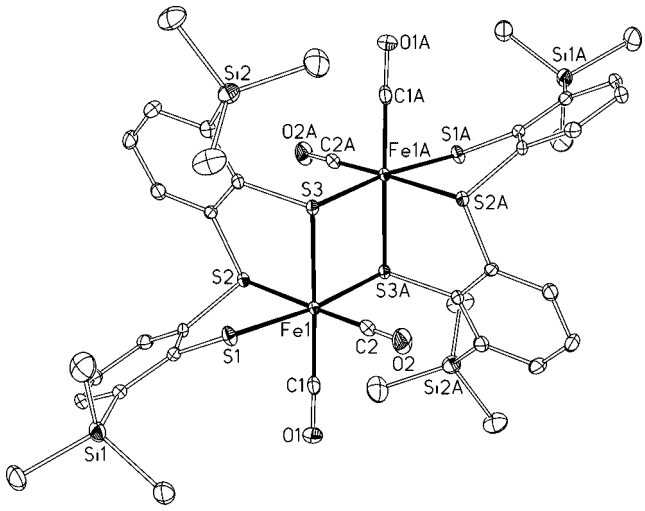

Figure 2. Molecular structure of **2** (50% thermal ellipsoids, H atoms and solvent molecules omitted).

Table 1. Selected bond lengths [pm] and angles [°] of **2** and **3**.

	2	**3**
Fe1–Fe1A[a]	341.51(6)	271.95(6)
Fe1–S1	230.55(6)	220.5(1)
Fe1–S2	227.91(6)	226.7(2)
Fe1–S3	229.64(6)	221.6(2)
Fe1–S3A[b]	233.65(6)	229.0(1)
Fe1–C1	179.5(2)	178.0(4)
Fe1–C2	178.1(2)	–
C1–O1	114.3(3)	114.1(4)
Fe1–S3–Fe1A[a]	94.97(2)	74.29(3)
S1–Fe1–S2	85.49(2)	88.06(4)
S2–Fe1–S3	87.92(2)	89.32(4)

[a] Fe1A in **2** = Fe2 in **3**. [b] S3A in **2** = S6 in **3**.

ments that are linked by thiolate bridges. The CO ligands and thioether donors are in axial positions with the two thiolate donors and iron atoms lying in the base plane. Due to the loss of a CO group the Fe–Fe distance in **3** [271.95(6) pm] decreases by 70 pm compared to that of **2** [341.51(6) pm].

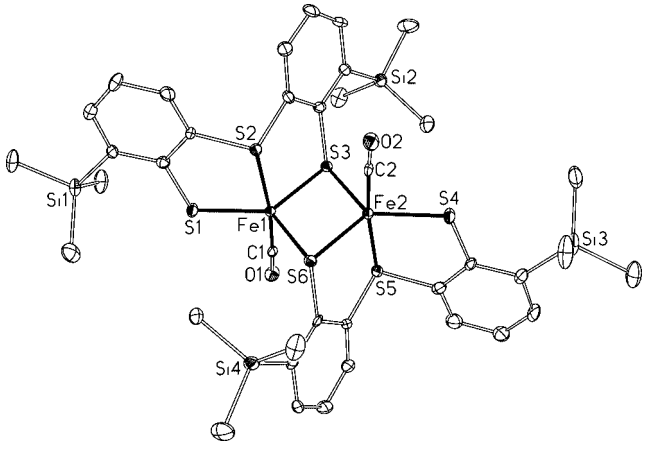

Figure 3. Molecular structure of **3** (50% thermal ellipsoids, H atoms and solvent molecules omitted).

When a solution of **3** in THF is either stirred under an atmosphere of CO for about 30 min or by bubbling of CO gas for about 2 min, compound **2** is formed again. The IR spectroscopic monitoring of the reaction confirmed that the ν(CO) band of **3** at 1975 cm^{-1} vanished and two bands at 2032 cm^{-1} and 1993 cm^{-1} appeared which correspond to the ν(CO) bands of **2**.

In analogy to the synthesis of **1**, complex **2** was treated with $[Ni(PMe_3)_2(‘S_2’)]$ in THF at 60 °C for about 4 h. During the course of the reaction, the green suspension turned into a dark-red solution. The IR spectrum of the solution showed a ν(CO) band at 1916 cm^{-1}. Treatment of the solution with methanol resulted in a black-grey microcrystalline material. The ^1H and ^{13}C NMR spectra of the isolated material (see Experimental Section) showed signals identical to those obtained for **1**. It did not show any signals for $SiMe_3$ groups, indicating the unique formation of **1**. An X-ray structure determination of a single crystal obtained from this material further corroborated this result. Thus, the formation of complex **1** via the ligand exchange type of reaction has unambiguously been proven.

Based upon this encouraging result we devised an alternative way of synthesizing **1** without using the ‘S_3’ ligand (Scheme 2). Treatment of $FeCl_2·4H_2O$ with two equivalents of deprotonated ‘S_2’$^{2-}$ in THF led to a red solution of $[Fe(‘S_2’)_2]^{2-}$ which was subsequently treated with PMe_3 and $Ni(BF_4)_2·6H_2O$. After addition of one more equivalent of ‘S_2’$^{2-}$ a slurry formed. Upon diffusion of CO gas into the slurry, a dark red solution formed gradually. The IR spectrum of the solution exhibited a ν(CO) band at 1916 cm^{-1}. Further work-up of the mixture afforded complex **1** in an isolable yield of 18%. It is noteworthy that a strict order of addition of the reactants is necessary for the formation of **1** in this one-pot synthesis.

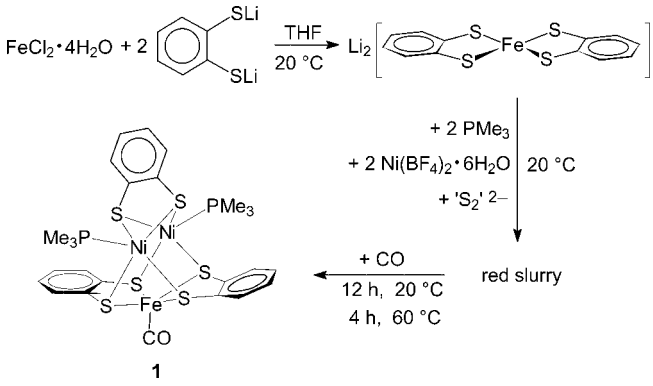

Scheme 2. Alternative synthesis of complex **1**.

DFT Calculations

Complex **1** readily reacts with protons to give dihydrogen and $[\mathbf{1}]^+$. When the solution of $[\mathbf{1}]^+$ is treated with hydride, the reduced complex **1** is formed again. Both complex **1** and its oxidation product $[\mathbf{1}]^+$ were characterized by single-crystal X-ray structure analysis.[11] In order to gain insight

Table 2. Comparison of selected bond lengths [pm] and angles [°] obtained experimentally and calculated theoretically for **1** and $[\mathbf{1}]^+$ along with the structural changes **Δ** upon oxidation. The average of experimental values which are symmetry-equivalent in the calculations is given.

	[1]		$[\mathbf{1}]^+$		**Δ**	
	Calcd.	Exp.	Calcd.	Exp.	Calcd.	Exp.
Fe1–S1/S2	223.6	221.9(1)	222.6	220.1(2)	–1.0	–1.8
Fe1–C1	173.6	173.8(5)	175.4	174.4(8)	+1.8	+ 0.6
Fe1–Ni1/Ni2	260.5	259.6(1)	259.7	258.3(2)	–0.8	–1.3
Ni1–Ni2	241.5	240.5(1)	246.0	243.1(2)	+4.5	+2.6
Ni1/Ni2–S2/S1	241.1	237.0(1)	237.6	232.6(2)	–3.5	–4.4
Ni1/Ni2–P1	221.2	220.3(2)	224.1	221.3(2)	+2.9	+1.0
Ni1/Ni2–S5	234.4	231.4(1)	232.7	229.2(2)	–1.7	–2.2
S1–Fe1–S2	90.26	90.00(4)	90.66	91.37(8)	+0.40	+1.37
S1–Fe1–S1A	84.76	84.01(5)	84.17	83.33(8)	–0.59	–0.68
S1–Fe1–S2A	155.96	154.24(5)	155.51	154.17(9)	–0.45	–0.07
Ni2–Fe1–Ni1	55.23	55.18(3)	56.54	56.14(3)	+1.31	+0.96
Ni2/Ni1–Ni1/Ni2–Fe1	62.39	62.41(3)	61.73	61.93(4)	–0.66	–0.48

into this redox process and to determine the details of the electronic structure, DFT calculations were carried out on cluster **1** and its cation $[\mathbf{1}]^+$. The symmetry has been constrained to C_{2v} for both the neutral and the oxidized cluster in all calculations. Therefore, one of the PMe_3 groups had to be rotated around the P–Ni bond as compared to the X-ray structures. Test calculations without symmetry constraints showed that the structures with C_{2v} symmetry are indeed lower in energy, thus legitimating this procedure.

As illustrated in Table 2, the theoretical structure determination (geometry optimization) yielded bond lengths and bond angles in very good agreement with the X-ray structure determination. For clarity, the molecular structure of **1** is depicted in Figure 4.

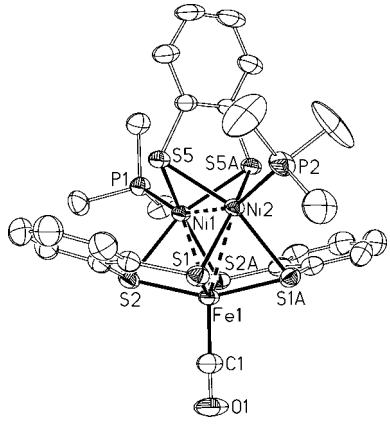

Figure 4. Molecular structure of **1** (50% thermal ellipsoids, H atoms and solvent molecules omitted, dashed lines represent the metal–metal distances).[11]

Differences in experimental bond lengths and bond angles, which are symmetry-equivalent in the DFT calculations, can be attributed to packing effects in the crystals. Therefore the data from the calculations were compared to the average value of these experimental bond lengths and angles. The plane defined by the 'S_2' ligand coordinating to the nickel atoms (denoted as 'S_2^{Ni}' in the following) and the axis of the CO ligand are slightly tilted in the experimental structures, while the calculations find a coplanar arrangement. However, it was found that the normal modes describing this movement are very low in both redox states of the cluster (around 50 cm^{-1}). Thus, such a distortion should be facile if a small force is exerted on the cluster due to the crystal environment. No significant change of the structural parameters upon oxidation of the cluster **1** is observed both for the experimental and the calculated structures. However, the trend of the changes of the structural parameters upon oxidation, e.g. slight elongation of the Ni1–Ni2 distance and shortening of the Ni1/Ni2–S2/S1 distance, is in general well reproduced by the calculations.

The calculation of the harmonic forcefield results in a frequency of 1955 cm^{-1} (exp. 1910 cm^{-1} in KBr/1916 cm^{-1} in CH_2Cl_2) for the ν(CO) band in **1**, and 1998 cm^{-1} (exp. 1952 cm^{-1} in KBr/1976 cm^{-1} in CH_2Cl_2) in $[\mathbf{1}]^+$. The experimentally observed blue-shift (42 cm^{-1} in KBr/60 cm^{-1} in CH_2Cl_2) upon oxidation is thus confirmed. The Kohn–Sham molecular orbitals were used for analyzing the electronic structure of our complexes. A stability analysis[14] of the restricted Hartree–Fock wavefunction of **1** showed that it is stable with respect to singlet and triplet instabilities. The S^2 value of 0.787 (S^2 = 0.75 for a doublet without spin contamination) in the unrestricted Hartree–Fock wave function of $[\mathbf{1}]^+$ does not indicate substantial multi-reference character for both compounds which would render such an analysis questionable. The results of several types of population analyses are summarized in Table 3. Note that the assignment of a charge to an atom within a polyatomic molecule cannot be carried out unambiguously. Different kinds of population analyses therefore will give different answers. It should be mentioned that the Mulliken population analysis[15] in particular is strongly dependent on the basis set and doubtful for an extended basis set, as far as absolute values of charges are concerned. Therefore, the common features of a Mulliken analysis, a natural population analysis (NPA),[16] and of a charge analysis based on generalized atomic polar tensors[17] are extracted. The latter is dependent on the basis set only implicitly by the way of the general quantum-mechanical description.

Table 3. Partial charges and d orbital occupations as calculated by various types of analysis of the density obtained in the DFT calculations. 'S_2^{Fe}' denotes the 'S_2' ligands coordinating to the iron atom, 'S_2^{Ni}' the 'S_2' ligand coordinating to the nickel atoms.

	1	$[\mathbf{1}]^+$ α+β	α-β
Mulliken population analysis			
Fe	–0.545	–0.569	–0.116
Ni	0.010	–0.030	0.315
S1/S2	–0.015	0.053	0.040
'S_2^{Fe}'	0.008	0.276	0.100
S5	–0.009	0.027	0.109
'S_2^{Ni}'	–0.223	0.026	0.301
PMe_3	0.302	0.425	–0.010
CO	0.129	0.201	0.003
d(Fe)	6.925	6.925	–0.104
d(Ni)	8.705	8.662	0.329
Natural Population Analysis			
Fe	–0.129	–0.135	–0.099
Ni	0.562	0.593	0.305
S1/S2	–0.012	0.046	0.042
'S_2^{Fe}'	–0.407	–0.168	0.104
S5	–0.115	–0.080	0.113
'S_2^{Ni}'	–0.727	–0.489	0.302
PMe_3	0.254	0.339	–0.009
CO	0.038	0.096	–0.004
d(Fe)	7.626	7.621	–0.096
d(Ni)	8.964	8.909	0.317
Charges from generalized atomic polar tensors			
Fe	–0.679	–0.672	–
Ni	–0.145	–0.021	–
S1/S2	–0.076	0.008	–
'S_2^{Fe}'	–0.171	0.082	–
S5	–0.019	–0.015	–
'S_2^{Ni}'	–0.041	0.048	–
PMe_3	0.443	0.486	–
CO	0.435	0.539	–

The oxidation states of iron and nickel (represented by their d occupations) do not change upon oxidation of **1** to $[\mathbf{1}]^+$. They are compatible with the formulation of Fe^{II} and Ni^{II}. This is consistent with the observation that only very small structural changes take place when **1** is oxidized to its cation. For example, the iron atom lies 4.95(1) pm above the plane defined by the atoms S1, S2, S1A and S2A in the crystal structure of **1**. Its distance from the plane defined by the atoms S1, S2, S3 and S4 in the crystal structure of $[\mathbf{1}]^+$ is with 4.98(2) pm almost identical, indicating that the iron center is not affected by the oxidation. The computed values for these distances in **1** and $[\mathbf{1}]^+$ coincide with the experimental data. No significant differences of the partial charges on any particular atoms are observed upon oxidation of the cluster. This means that the positive charge in $[\mathbf{1}]^+$ cannot be assigned to individual atoms but is distributed over the whole cluster. What at first seems surprising is the fact that no charge ends up on the metal centers. However, this is in line with the negligible changes in the d level occupation. On the other hand the partial charges on all ligands are increased upon oxidation. Thus, main parts of the positive charge in $[\mathbf{1}]^+$ are residing on the 'S_2' ligands.

The picture is very different for the spin polarization. As opposed to the positive charge, the unpaired electron is confined to a more restricted region of the molecule. A small negative spin polarization arises at the iron atom, but the main part of the spin polarization is located on the Ni_2'S_2^{Ni}' fragment of the cluster. About two thirds of the magnetic moment are located on the nickel d orbitals and about one third on the 'S_2^{Ni}' ligand. Approximately two thirds of the spin polarization on the 'S_2^{Ni}' ligand are located on the thiolate donor functions. This data can be very nicely visualized by an analysis of the molecular orbitals. Upon oxidation an electron is removed from the HOMO of **1** which has essentially the same form as the SOMO in $[\mathbf{1}]^+$ and is mainly formed from d orbitals on the nickel atoms and p orbitals on the adjacent sulfur atoms (Figure 5). The localization of the unpaired electron at these atoms with a small contribution at the iron atom can be clearly seen from a plot of the spin density of $[\mathbf{1}]^+$ (Figure 6). These findings are consistent with EPR measurements, which have been reported in ref.[11]

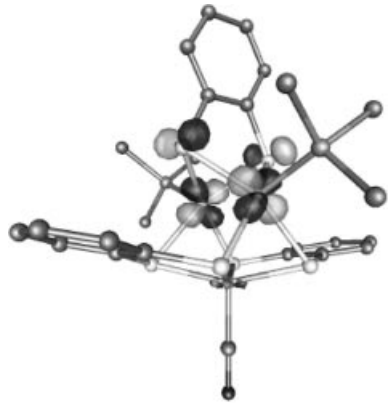

Figure 5. Plot of the highest occupied molecular orbital (HOMO) of **1** (H atoms omitted).

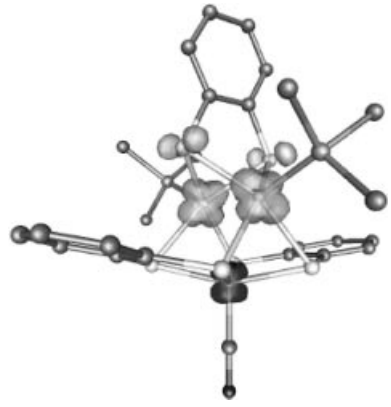

Figure 6. Plot of the spin density in $[\mathbf{1}]^+$ (H atoms omitted).

At first this localization of the spin density on the nickel atoms and the adjacent sulfur atoms seems to be contradictory to the above described delocalization of the positive charge in $[\mathbf{1}]^+$. Things become clear, however, if we imagine the oxidation as a two-step procedure. In the first step an electron is removed from the HOMO, which leaves an *unpaired* electron in an orbital located mainly at the nickel and adjacent sulfur atoms. At the same time the electronic

structure of the complex cation relaxes and a substantial donation of *paired* electrons from the 'S_2' ligands takes place to compensate for the lack of electrons on the metal centers. Thus, the 'S_2' ligands serve as a kind of electron density reservoir, which prevent the buildup of positive charge on the nickel atoms upon removal of one electron.

Constant Potential Coulometry

The cyclic voltammogram of **1** (given in ref.[11]) exhibits three quasi-reversible one-electron waves at –1.071, –0.095, and 0.844 V relative to NHE, which are assigned to the redox couples $\mathbf{1}^{0/-}$, $\mathbf{1}^{0/+}$, and $\mathbf{1}^{+/2+}$, respectively.[11] The potential of the second wave lies within the range which has been observed for several [NiFe] hydrogenase redox reactions.[3c,5d] In addition, the small difference in the X-ray structure parameters of **1** and $[\mathbf{1}]^+$ suggests that the electron transfer should be quite fast as a result of a low reorganization barrier. This exciting result prompted us to check the ability of **1** in catalyzing the reduction of H^+ to H_2 by constant potential coulometry. A solution of 3.2 mmol of HBF_4 in CH_2Cl_2 was electrolyzed in the presence of 0.1 mmol of **1** by a platinum electrode at –0.48 V relative to NHE for 2 h. Interestingly, the number of coulombs increases with time (Figure 7). H_2 gas evolution was observed during the electrolysis. Samples of the gas phase were taken at 0, 1 and 2 h of electrolysis, and the amount of the formation of H_2 was estimated by gas chromatography. After the end of 1 and 2 h of electrolysis 0.09 ± 0.004 and 0.15 ± 0.004 mmol of H_2 was detected, respectively. When the electrolysis was performed under identical conditions but in the absence of the complex, the number of coulombs did not increase with time and no H_2 formation was observed. The IR spectrum of the electrolyzed solution exhibited the CO band at 1917 cm^{-1}, which confirmed that the CO molecule did not dissociate during electrolysis. These results suggest that complex **1** is capable of mediating the reaction. But, the amount of charge transferred is nearly twice as high as the corresponding amount of H_2 produced, which indicates that some side reaction takes place. Nevertheless, **1** seems to be the first [NiFe] complex that mediates the reduction of protons to H_2 at a very mild reduction potential. Efforts are needed to optimize the coulometric experimental conditions.

The exact site of **1** where the proton initially interacts and is reduced to H_2 is not yet been understood. The reaction may either be preceded via an initial formation of a protonated thiolate species or via a Ni^{III}–H like intermediate.[18] According to the DFT studies on **1** and $[\mathbf{1}]^+$, an initial formation of a protonated thiolate species (at the nickel centers) is fairly reasonable, because the HOMO has also a large amplitude on the thiolate donor atoms adjacent to the nickel atoms. Furthermore, a considerable part of the spin density of the oxidized cluster is located on these atoms.

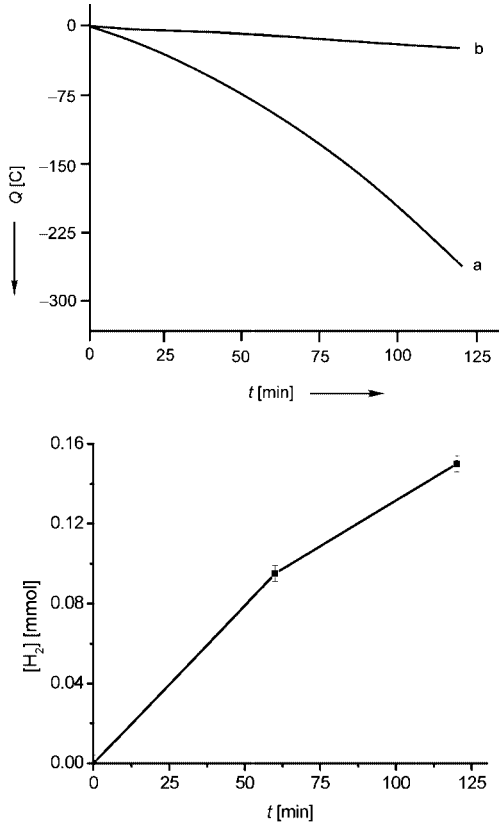

Figure 7. Top: plot of number of coulombs vs. electrolysis time in the presence (a) and in the absence (b) of complex **1**. Bottom: plot of mmols of H_2 produced per mmol of **1** vs. electrolysis time.

Conclusions

The formation of **1** from the reaction between $[Fe(CO)_2('S_3')]_2$ and $[Ni(PMe_3)_2('S_2')]$ was not understood up to now. Through the synthesis of a silylated precursor $[Fe(CO)_2(^{si}S_3)]_2$ (**2**), an earlier observation of the formation of **1** from $[Fe(CO)_2('S_3')]_2$ and $[Ni(PMe_3)_2('S_2')]$ is now understood to be a ligand exchange process. Based on this result, an alternative route for the synthesis of **1** in a one-pot reaction has been developed. The reported trinuclear [NiFe] complex **1** readily reduces protons to H_2 and in turn undergoes oxidation to form $[\mathbf{1}]^+$. DFT calculations suggest that the oxidation states of the metal centers are Fe^{II} and Ni^{II} and do not change upon oxidation of **1** to $[\mathbf{1}]^+$. The unpaired electron in $[\mathbf{1}]^+$ is located to a large extent on the nickel atoms and the adjacent thiolate donor functions. The charge, however, is distributed over the whole cluster and main parts reside on the 'S_2' ligands. These results are compatible with the protonation of a thiolate group as a first step of the reduction mechanism. Preliminary constant potential coulometric results indicate that the trinuclear model complex has catalytic activity for proton reduction under mild potential.

Experimental Section

General: Unless noted otherwise, all manipulations were carried out in absolute solvents under exclusion of air using standard Schlenk techniques. IR spectra of solutions were recorded in CaF_2

cuvettes with compensation of the solvent bands, and solids were measured as KBr pellets. NMR spectra were recorded at room temperature and chemical shifts are quoted in δ scale (downfield shifts positive) with the residual signals of the deuterated solvent used as an internal reference. Mass spectra were measured in the field desorption (FD) or fast atom bombardment (FAB) mode. Physical measurements were carried out with the following instruments: IR: Perkin–Elmer 983, Perkin–Elmer 1600 FTIR, and Perkin–Elmer 16PC FTIR; NMR: JEOL FT-JNM-GX 270, Lambda LA 400. MS: JEOL MSTATION 700. Constant Potential Coulometry: Experiments were performed on Autolab Potentiostat/Galvanostat equipped with a personal computer. A coulometric cell assembly consisting of a Pt-gauge working electrode, a platinum wire counter electrode, and a 1 M SCE reference electrode was used. The reference and counter electrodes were separated from the experimental solution by a glass frit. This closed cell assembly (total cell volume of 310 mL) provides with a probe for sampling. This was fitted with a rubber septum and the gas samples were taken before, during, and at the end of the electrolysis. The amount of H_2 gas produced during electrolysis was detected by gas chromatography. The compounds 1,2-Benzenedithiol ('S_2'–H_2),[19] [Fe(bda)$(CO)_3$],[20] PMe_3,[21] bis(2-mercapto-3-trimethylsilylphenyl) sulfide(2–) ($^{si}S_3$–H_2),[22] and $(NMe_4)_2$[Fe$(CO)_2$('S_2')$_2$][13] were prepared according the literature methods.

[Fe$(CO)_2$($^{si}S_3$)]$_2$ (2): All manipulations were carried out under CO atmosphere. To a solution of [Fe(bda)$(CO)_3$] (716 mg, 2.503 mmol) in THF (5 mL) a solution of $^{si}S_3$–H_2 (974 mg, 2.473 mmol) in THF (5 mL) was added. A gas evolution was observed and the solution color changed to dark-green. This solution was kept at 20 °C. The black green microcrystal that formed after 15 d, were separated from the mother liquor and dried with a stream of CO. Yield: 250 mg (17.5%); $C_{40}H_{48}Fe_2O_4S_6Si_4$·2THF (1153.46): calcd. C 49.98, H 5.59, S 16.68; found C 50.43, H 5.93, S 16.67. IR (KBr): $\tilde{\nu}$ = 2029, 1988 (CO) cm^{-1}. Due to the lability of **2** in solution, NMR spectra that were readily analyzed could not be obtained.

[('S_2')$_2$Ni(PMe_3)}$_2$Fe(CO)('S_2')$_2$] (1) Starting from 2: A THF suspension (30 mL) of a mixture of **2** (630 mg, 0.624 mmol) and [Ni$(PMe_3)_2$('S_2')] (436 mg, 1.220 mmol) was stirred at 60 °C for 4 h. During the course of time, the suspension changed to a clear dark-red solution. This was filtered, and treated with MeOH (240 mL). Black-grey microcrystals precipitated, were removed after 24 h, washed with MeOH (15 mL) and dried in vacuo. Yield: 90 mg (19%). IR (KBr): $\tilde{\nu}$ = 1910 (CO) cm^{-1}. IR (CH_2Cl_2): $\tilde{\nu}$ = 1916 (CO) cm^{-1}. ^{1}H NMR (269.6 MHz, CD_2Cl_2): δ = 7.33 (m, 4 H, C_6H_4), 6.81 (m, 4 H, C_6H_4), 6.67 (m, 2 H, C_6H_4), 6.33 (m, 2 H, C_6H_4), 1.97 (s, 18 H, PC_3H_9) ppm. ^{13}C{^{1}H} NMR (100.4 MHz, CD_2Cl_2): δ = 207.3 (CO), 146.7, 131.0, 130.3, 125.2, 123.4, (C_6H_4), 18.2 (PMe_3) ppm. ^{31}P{^{1}H} NMR (161.7 MHz, CD_2Cl_2): δ = 214.6 (PMe_3) ppm. $C_{25}H_{30}FeNi_2OP_2S_6$ (744.09): calcd. C 38.79, H 3.91, S 24.85; found C 38.54, H 3.82, S 24.80.

Alternative Synthesis of 1: To a suspension of $FeCl_2$·$4H_2O$ (200 mg, 1.001 mmol) in THF (10 mL) a solution of 'S_2'–H_2 (0.23 mL, 2.001 mmol) and BuLi (2.5 M in *n*-hexane, 1.61 mL, 4.025 mmol) in THF (10 mL) was added. The resulting red solution was treated with PMe_3 (0.21 mL, 2.04 mmol) and then with a solution of $Ni(BF_4)_2$·$6H_2O$ (684 mg, 2.001 mmol) in THF (15 mL). To this mixture again a solution of 'S_2'–H_2 (0.12 mL, 1.046 mmol) and BuLi (2.5 M in *n*-hexane, 0.81 mL, 2.025 mmol) in THF (10 mL) was added. A slurry was formed, to this, additional THF (75 mL) was added. Then the Schlenk tube was fitted with a septum. CO gas (60 mL, 2.68 mmol) was allowed to diffuse slowly into the mixture, and the solution was stirred vigorously at 20 °C for 15 h. During the course, the suspension was changed to a clear solution, which was stirred again at 60 °C for 4 h. Half of the solvent was evaporated, the solution was filtered and MeOH (140 mL) was added. Black-grey microcrystals formed, were filtered, washed with MeOH (25 mL) and dried in vacuo. Yield: 140 mg (18%). Characterization: similar as above.

Density Functional Theory (DFT) Calculations: The DFT modules of the program package Turbomole[23] were used and the BP86 exchange-correlation functional[24] with a triple-zeta valence-polarized Gaussian basis set[25] was employed for all calculations. The resolution of identity (RI) technique[26] was employed to accelerate the calculations. The natural population analysis (NPA) [16] was done with Gaussian98[27] employing the Kohn–Sham molecular orbitals obtained from the Turbomole calculations. The program gOpenmol[28] was used for the visualizations (Figure 5 and Figure 6). All structures were fully optimized and characterized as true minima on the potential energy hypersurface by means of a vibrational analysis. Accurately converged SCF results (a termination threshold of at least 10^{-8} a.u. for the total energy) were used to guarantee satisfactory accuracy in the force constant calculations. The force constants were obtained as numerical first derivatives of the analytical energy gradients as implemented in the parallel PVM code SNF.[29]

Constant Potential Coulometry: In a typical experiment, a coulometric cell (320 mL capacity) containing a solution of **1** (80 mg, 0.103 mmol) in CH_2Cl_2 (100 mL), HBF_4 (54% solution in Et_2O, 5 mL, 3.2 mmol) and NBu_4PF_6 (3.874 g, 10 mmol) was electrolyzed at –0.15 V vs. 0.1 M SCE for 2 h (25 μL gas samples were taken from the cell at every hour intervals) and the formation of H_2 gas was analyzed by GC (TC detector, retention time: 0.733 s). An identical experiment without **1** was also performed.

X-Ray Structure Determination of [Fe$(CO)_2$($^{si}S_3$)]$_2$·2THF (2·2THF) and [Fe(CO)($^{si}S_3$)]$_2$·3THF (3·3THF): Suitable single crystals were embedded in protective perfluoro polyether oil. Data were collected at 100 K on a Bruker–Nonius KappaCCD diffractometer using Mo-K_α radiation (λ = 71.073 pm), and a graphite monochromator. A numerical absorption correction was applied.[30] for **2**·2THF, while for **3**·3THF a semiempirical absorption correction based on multiple scans was performed (SADABS).[31] The structures were solved by direct methods; full-matrix least-squares refinement was carried out on F^2 using SHELXTL NT 6.12.[32] All non-hydrogen atoms were refined anisotropically. All hydrogen atoms were geometrically positioned; their isotropic displacement parameters were tied to those of their corresponding carrier atoms by a factor of 1.2 or 1.5. In the case of **3**·3THF there is pseudosymmetry which emulates a *Pccn* unit cell, but is not fully supported by the diffraction pattern which is consistent with the correct space group $P2_12_12$. The Flack parameter of approx. 0.5 suggests a centrosymmetric space group, though. A solution of the structure in *Pccn* is possible, but the subsequent refinement results in a dramatical increase of all *R*-values and estimated standard deviations. Therefore, the presence of an inversion twin is the best explanation and consistent with the experimental data. One of the three THF solvent molecules present in the asymmetric unit is disordered on two different crystallographic twofold axes. This disordered solvent molecule has been refined using constraints and no hydrogen atoms have been introduced for it. Selected crystallographic data are summarized in Table 4.

CCDC-608118 and -608119 contain the supplementary crystallographic data for this paper. These data can be obtained free of charge from The Cambridge Crystallographic Data Centre via www.ccdc.cam.ac.uk/data_request/cif.

Table 4. Selected crystallographic data for **2**·2THF and **3**·3THF.

Compound	**2**·2THF	**3**·3THF
Formula	$C_{48}H_{64}Fe_2O_6S_6Si_4$	$C_{50}H_{72}Fe_2O_5S_6Si_4$
M_r [g mol^{-1}]	1153.41	1169.50
Crystal system	triclinic	orthorhombic
Space group	$P\bar{1}$	$P2_12_12$
a [pm]	971.05(5)	2117.5(3)
b [pm]	1155.9(1)	27.526(4)
c [pm]	1358.4(2)	982.7(1)
α [°]	103.238(7)	90
β [°]	99.060(5)	90
γ [°]	103.119(6)	90
V [nm^3]	1.4097(3)	5.7278(13)
Z	1	4
ρ_{calcd}[g cm^{-3}]	1.359	1.356
μ[mm^{-1}]	0.865	0.852
Crystal size [mm^3]	$0.35 \times 0.32 \times 0.14$	$0.32 \times 0.23 \times 0.08$
$T_{min.}/T_{max.}$	0.764/0.898	0.756/0.934
Measured reflections	34052	39756
Independent reflections	6715	13148
Observed reflections[a]	5335	9953
Refined parameters	304	635
Largest diff. peak and hole [e nm^{-3}]	585/–640	438/–420
$R1$[a]; wR_2[b] (%)	3.58; 8.76	4.47; 8.60

[a] [$I > 2\sigma(I)$]. [b] All data.

Acknowledgments

We gratefully acknowledge the financial support provided by the Deutsche Forschungsgemeinschaft (DFG), Sonderforschungsbereich (SFB-583) and the Fonds der Chemischen Industrie.

[1] a) P. M. Vignais, B. Billoud, J. Meyer, *FEMS Microbiol. Rev.* **2001**, *25*, 455–501; b) R. K. Thauer, A. R. Klein, G. C. Hartmann, *Chem. Rev.* **1996**, *96*, 3031–3042; c) S. P. J. Albracht, *Biochim. Biophys. Acta* **1994**, *1188*, 167–204; d) T. Lissolo, S. Pulvin, D. Thomas, *J. Biol. Chem.* **1984**, *259*, 11725–11729; e) M. W. W. Adams, L. E. Mortenson, J.-S. Chen, *Biochim. Biophys. Acta* **1980**, *594*, 105–176.

[2] V. Artero, M. Fontecave, *Coord. Chem. Rev.* **2005**, *249*, 1518–1554.

[3] a) A. Volbeda, M. H. Charon, C. Piras, E. C. Hatchikian, M. Frey, J. C. Fontecilla-Camps, *Nature* **1995**, *373*, 580–587; b) A. Volbeda, E. Garcin, A. L. de Lacey, V. M. Fernandes, E. C. Hatchikian, M. Frey, J. C. Fontecilla-Camps, *J. Am. Chem. Soc.* **1996**, *118*, 12989–12996; c) M. Frey, *Struct. Bonding (Berlin)* **1998**, *90*, 97–126; d) Y. Higuchi, H. Ogata, K. Miki, N. Yasuoka, T. Yagi, *Structure* **1999**, *7*, 549–556.

[4] a) J. W. Peters, W. N. Lanzilotta, B. J. Lemon, L. C. Seefeldt, *Science* **1998**, *282*, 1853–1858; b) Y. Nicolet, C. Piras, P. Legrand, C. E. Hatchikian, J. C. Fontecilla-Camps, *Structure* **1999**, *7*, 13–23.

[5] a) Z. J. Gu, J. Dong, C. B. Allan, S. B. Choudhury, R. Franco, J. J. G. Moura, I. Moura, J. LeGall, A. E. Przybyla, W. Roseboom, S. P. J. Albracht, M. J. Axley, R. A. Scott, M. J. Maroney, *J. Am. Chem. Soc.* **1996**, *118*, 11155–11165; b) A. L. de Lacey, E. C. Hatchikian, A. Volbeda, M. Frey, J. C. Fontecilla-Camps, V. M. Fernandez, *J. Am. Chem. Soc.* **1997**, *119*, 7181–7189; c) Y. Montet, P. Amara, A. Volbeda, X. Vernede, E. C. Hatchikian, M. J. Field, M. Frey, J. C. Fontecilla-Camps, *Nat. Struct. Biol.* **1997**, *4*, 523–526; d) A. K. Jones, S. E. Lamle, H. R. Pershad, K. A. Vincent, A. P. J. Albracht, F. A. Amstrong, *J. Am. Chem. Soc.* **2003**, *125*, 8505–8524; e) M. Brecht, M. van Gastel, T. Buhrke, B. Friedrich, W. Lubitz, *J. Am. Chem. Soc.* **2003**, *125*, 13075–13083.

[6] a) *The Bioinorganic Chemistry of Nickel* (Ed.: J. R. Lancaster Jr), VCH, Weinheim, **1988**; b) J. C. Fontecilla-Camps, *Struct. Bond.* **1998**, *91*, 1–29; c) M. Frey, *Struct. Bonding (Berlin)* **1998**, *90*, 97–126; d) R. Cammack, *Nature* **1999**, *397*, 214–215; e) M. W. W. Adams, E. I. Stiefel, *Science* **1998**, *282*, 1842–1843; f) M. J. Maroney, G. Davidson, C. B. Allan, J. Figlar, *Struct. Bonding (Berlin)* **1998**, *92*, 2–65.

[7] a) S. Foerster, M. Stein, M. Brecht, H. Ogata, Y. Higutchi, W. Lubitz, *J. Am. Chem. Soc.* **2003**, *125*, 83–93; b) H.-J. Fan, M. B. Hall, *J. Am. Chem. Soc.* **2002**, *124*, 394–395, and references cited therein; c) P. E. M. Siegbahn, M. R. A. Blomberg, M. Wirstam née Pavlov, R. H. Crabtree, *J. Biol. Inorg. Chem.* **2001**, *6*, 460–466, and references therein.

[8] a) M. Y. Darensbourg, E. J. Lyon, J. J. Smee, *Coord. Chem. Rev.* **2000**, 553–561; b) A. C. Marr, D. J. E. Spencer, M. Schröder, *Coord. Chem. Rev.* **2001**, *219*, 1055–1074; c) D. J. Evans, C. J. Pickett, *Chem. Soc. Rev.* **2003**, *32*, 268–275; d) E. Bouwman, J. Reedijk, *Coord. Chem. Rev.* **2005**, *249*, 1555–1581.

[9] a) S. Ciurli, S.-B. Yu, R. H. Holm, K. K. P. Srivastava, E. Munck, *J. Am. Chem. Soc.* **1990**, *112*, 8169–8171; b) W. Saak, S. Pohl, *Angew. Chem.* **1991**, *103*, 869–870; *Angew. Chem. Int. Ed. Engl.* **1991**, *30*, 881–883; c) J. Zhou, M. J. Scott, Z. Hu, G. Peng, E. Munck, R. H. Holm, *J. Am. Chem. Soc.* **1992**, *114*, 10843–10854; d) C. Junghams, W. Saak, S. Pohl, *J. Chem. Soc. Chem. Commun.* **1994**, 2327–2328; e) R. L. Holliday, L. C. Roof, B. Hargus, D. M. Smith, P. T. Wood, W. T. Pennington, J. W. Kolis, *Inorg. Chem.* **1995**, *34*, 4392–4401; f) C. H. Lai, J. H. Reibenspies, M. Y. Darensbourg, *Angew. Chem.* **1996**, *108*, 2551–2554; *Angew. Chem. Int. Ed. Engl.* **1996**, *35*, 2390–2393; g) F. Osterloh, W. Saak, S. Pohl, *J. Am. Chem. Soc.* **1997**, *119*, 5648–5656; h) E. Bouwman, R. K. Henderson, A. L. Spek, J. Reedijk, *Eur. J. Inorg. Chem.* **1999**, *4*, 217–219; i) S. C. Davies, D. J. Evans, D. L. Hughes, S. Longhurst, J. R. Sanders, *Chem. Commun.* **1999**, 1935–1936; j) T. Glaser, T. Beissel, E. Bill, T. Weyhermüller, V. Schünemann, W. Meyer-Klaucke, A. X. Trautwein, K. Wieghardt, *J. Am. Chem. Soc.* **1999**, *121*, 2193–2208; k) G. Steinfeld, B. Kersting, *Chem. Commun.* **2000**, 205–206; l) M. Razavet, S. C. Davis, D. L. Hughes, C. J. Pickett, *Chem. Commun.* **2001**, 847–848; m) M.-C. Chalbot, A. M. Mills, A. L. Spek, G. J. Long, E. Bouwman, *Eur. J. Inorg. Chem.* **2003**, 453–457; n) M. C. Smith, J. E. Barclay, S. P. Cramer, S. C. Davies, W.-W. Gu, D. L. Hughes, S. Longhurst, D. J. Evans, *J. Chem. Soc. Dalton Trans.* **2002**, 2641–3647; o) D. Sellmann, F. Geipel, F. Lauderbach, F. W. Heinemann, *Angew.*

Chem. **2002**, *114*, 654–656; *Angew. Chem. Int. Ed.* **2002**, *41*, 632–634; p) M. C. Smith, J. E. Barclay, S. C. Davies, D. L. Hughes, D. J. Evans, *Dalton Trans.* **2003**, 4147–4151; q) D. Sellmann, R. Prakash, F. W. Heinemann, M. Moll, M. Klimowicz, *Angew. Chem.* **2004**, *116*, 1913–1916; *Angew. Chem. Int. Ed.* **2004**, *43*, 1877–1880; r) P. A. Stenson, A. Martin-Becerra, C. Wilson, A. J. Blake, J. McMaster, M. Schröder, *Chem. Commun.* **2006**, 317–319.

[10] Z. Li, Y. Ohki, K. Tatsumi, *J. Am. Chem. Soc.* **2005**, *127*, 8950–8951.

[11] D. Sellmann, F. Lauderbach, F. Geipel, F. W. Heinemann, M. Moll, *Angew. Chem.* **2004**, *116*, 3203–3206; *Angew. Chem. Int. Ed.* **2004**, *43*, 3141–3144.

[12] D. Sellmann, J. Sutter, *Prog. Inorg. Chem.* **2003**, *52*, 585–681.

[13] D. Sellmann, F. Geipel, F. Lauderbach, F. W. Heinemann, *Chem. Eur. J.* **2002**, *8*, 958–966.

[14] R. Bauernschmitt, R. Ahlrichs, *J. Chem. Phys.* **1996**, *104*, 9047–9052.

[15] a) R. S. Mulliken, *J. Chem. Phys.* **1955**, *23*, 1833–1840; b) R. S. Mulliken, *J. Chem. Phys.* **1955**, *23*, 1841–1846.

[16] A. E. Reed, R. B. Weinstock, F. Weinhold, *J. Chem. Phys.* **1985**, *83*, 735–746.

[17] J. Cioslowski, *J. Am. Chem. Soc.* **1989**, *111*, 8333–8336.

[18] V. Grass, D. Lexa, J.-M. Savéant, *J. Am. Chem. Soc.* **1997**, *119*, 7526–7532.

[19] J. Degani, R. Fochi, *Synthesis* **1976**, *7*, 471–472.

[20] A. J. P. Domingos, J. A. S. Howell, B. F. G. Johnson, J. Lewis, *Inorg. Synth.* **1990**, *28*, 52–55.

[21] W. Wolfsberger, H. Schmidbaur, *Synth. React., Inorg. Met.-Org. Chem.* **1974**, *4*, 149–156.

[22] D. Sellmann, R. Prakash, F. Geipel, F. W. Heinemann, *Eur. J. Inorg. Chem.* **2002**, 2138–2146.

[23] a) R. Ahlrichs, M. Bär, M. Häser, H. Horn, C. Kölmel, *Chem. Phys. Lett.* **1989**, *162*, 165–169; b) O. Treutler, R. Ahlrichs, *J. Chem. Phys.* **1995**, *102*, 346–354.

[24] a) A. D. Becke, *Phys. Rev. A* **1988**, *38*, 3098–3100; b) J. P. Perdew, *Phys. Rev. B* **1986**, *33*, 8822–8824; c) S. H. Vosko, L. Wilk, M. Nusair, *Can. J. Phys.* **1980**, *58*, 1200–1211.

[25] A. Schäfer, C. Huber, R. Ahlrichs, *J. Chem. Phys.* **1994**, *100*, 5829–5835.

[26] K. Eichkorn, F. Weigend, O. Treutler, R. Ahlrichs, *Theor. Chem. Acc.* **1997**, *97*, 119–124.

[27] *Gaussian 98*, Revision A.11.3, M. J. Frisch, G. W. Trucks, H. B. Schlegel, G. E. Scuseria, M. A. Robb, J. R. Cheeseman, V. G. Zakrzewski, J. A. Montgomery Jr, R. E. Stratmann, J. C. Burant, S. Dapprich, J. Millam, A. D. Daniels, K. N. Kudin, M. C. Strain, O. Farkas, J. Tomasi, V. Barone, M. Cossi, R. Cammi, B. Mennucci, C. Pomelli, C. Adamo, S. Clifford, J. Ochterski, G. A. Petersson, P. Y. Ayala, Q. Cui, K. Morokuma, N. Rega, P. Salvador, J. J. Dannenberg, D. K. Malick, A. D. Rabuck, K. Raghavachari, J. B. Foresman, J. Cioslowski, J. V. Ortiz, A. G. Baboul, B. B. Stefanov, G. Liu, A. Liashenko, P. Piskorz, I. Komaromi, R. Gomperts, R. L. Martin, D. J. Fox, T. Keith, M. A. Al-Laham, C. Y. Peng, A. Nanayakkara, M. Challacombe, P. M. W. Gill, B. Johnson, W. Chen, M. W. Wong, J. L. Andres, C. Gonzalez, M. Head-Gordon, E. S. Replogle, J. A. Pople, Gaussian, Inc., Pittsburgh PA, **2002**.

[28] a) L. Laaksonen, *J. Mol. Graphics Modell.* **1992**, *10*, 33–34; b) D. L. Bergman, L. Laaksonen, A. Laaksonen, *J. Mol. Graphics Modell.* **1997**, *15*, 301–306.

[29] a) C. Kind, M. Reiher, J. Neugebauer, B. A. Hess, *SNF,* Universität Erlangen-Nürnberg, **1999–2000**; b) J. Neugebauer, M. Reiher, C. Kind, B. A. Hess, *J. Comput. Chem.* **2002**, *23*, 895–910.

[30] P. Coppens, *Crystallographic Computing (Copenhagen).* **1970**, 225–270.

[31] *SADABS* 2.06, Bruker AXS, Inc., Madison, WI, **2002**.

[32] *SHELXTL* NT 6.12, Bruker AXS, Inc., Madison, WI, **2002**.

Received: November 16, 2006
Published Online: May 29, 2007

